Analysis of Magnetohydrodynamic Perturbations in the Radial-field Solar Wind from *Parker Solar Probe* Observations

Siqi Zhao[1,2], Huirong Yan[1,2,*], Terry Z. Liu[3], Mingzhe Liu[4], Mijie Shi[5]

[1]*Deutsches Elektronen Synchrotron DESY, Germany*
[2]*Institut für Physik und Astronomie, Universität Potsdam, Germany*
[3]*Department of Earth, Planetary, and Space Sciences, University of California, USA*
[4]*LESIA, Observatoire de Paris, Université de Paris, France*
[5]*Institute of Space Sciences, Shandong University, China*

siqi.zhao@desy.de

Mode composition in MHD perturbations

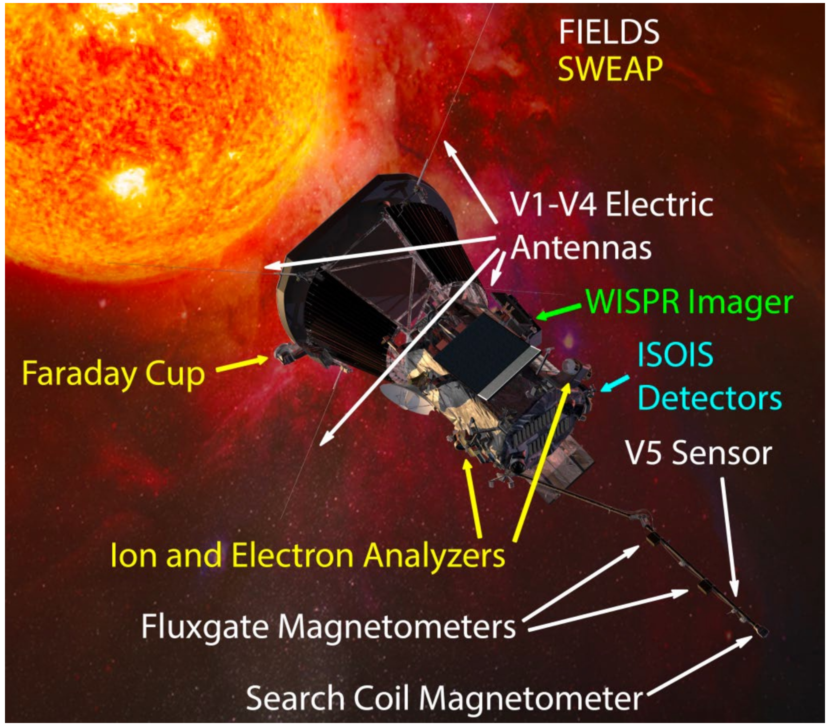

[Parker Solar Probe and Instrumentations.
Credits: UC Berkeley Website]

- Launch Date: August 12th, 2018.
- Orbit Design: perihelia decrease from 35.7 to 9.86 $R_{\odot}$.

- Solar wind provides an excellent laboratory for studying ubiquitous plasma turbulence from magnetohydrodynamic (MHD) to kinetic scales (e.g., Verscharen et al. 2019).

- MHD perturbations can be decomposed into three types of linear eigenmodes: **Alfvén**, **fast**, and **slow** modes (e.g., Glassmeier et al. 1995).

Part I

Mode composition in MHD perturbations

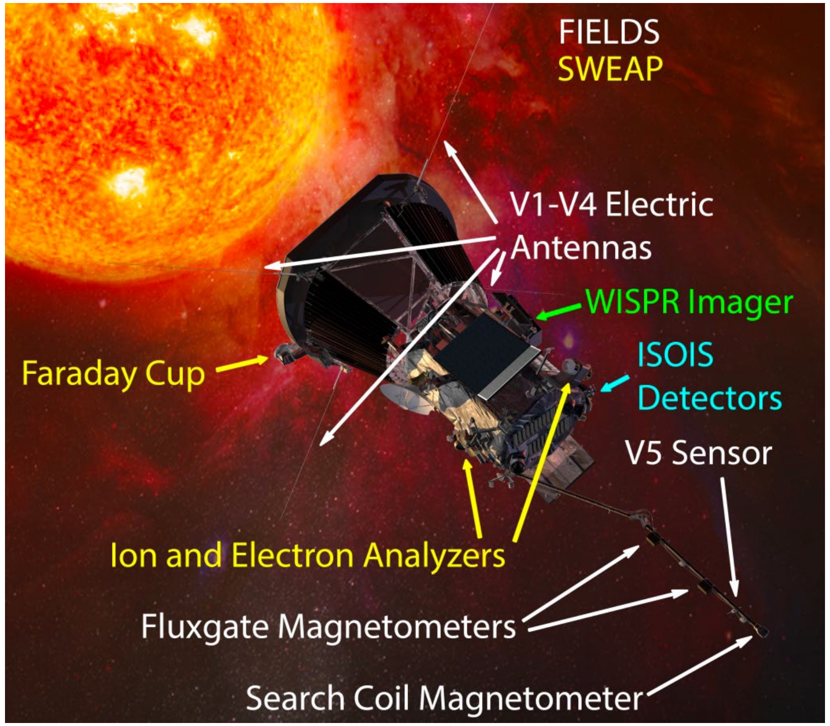

[Parker Solar Probe and Instrumentations. Credits: UC Berkeley Website]

- Launch Date: August 12th, 2018.
- Orbit Design: perihelia decrease from 35.7 to 9.86 $R_{\odot}$.

- In the inertial scale, perturbations are composed of incompressible and compressible perturbations.

~90%; Alfvén modes

The nature remains uncertain.

Magnetic compression is often associated with slow modes, whereas fast modes are often neglected.
e.g., $\delta B_{\perp}$ arise from Alfvén mode and $\delta B_{\parallel}$ totally from slow mode (Chen et al. 2020).

Whether is the assumption of $\delta B_{\parallel}$ totally from slow modes always valid?

Mode decomposition

Part II An overview of a representative case

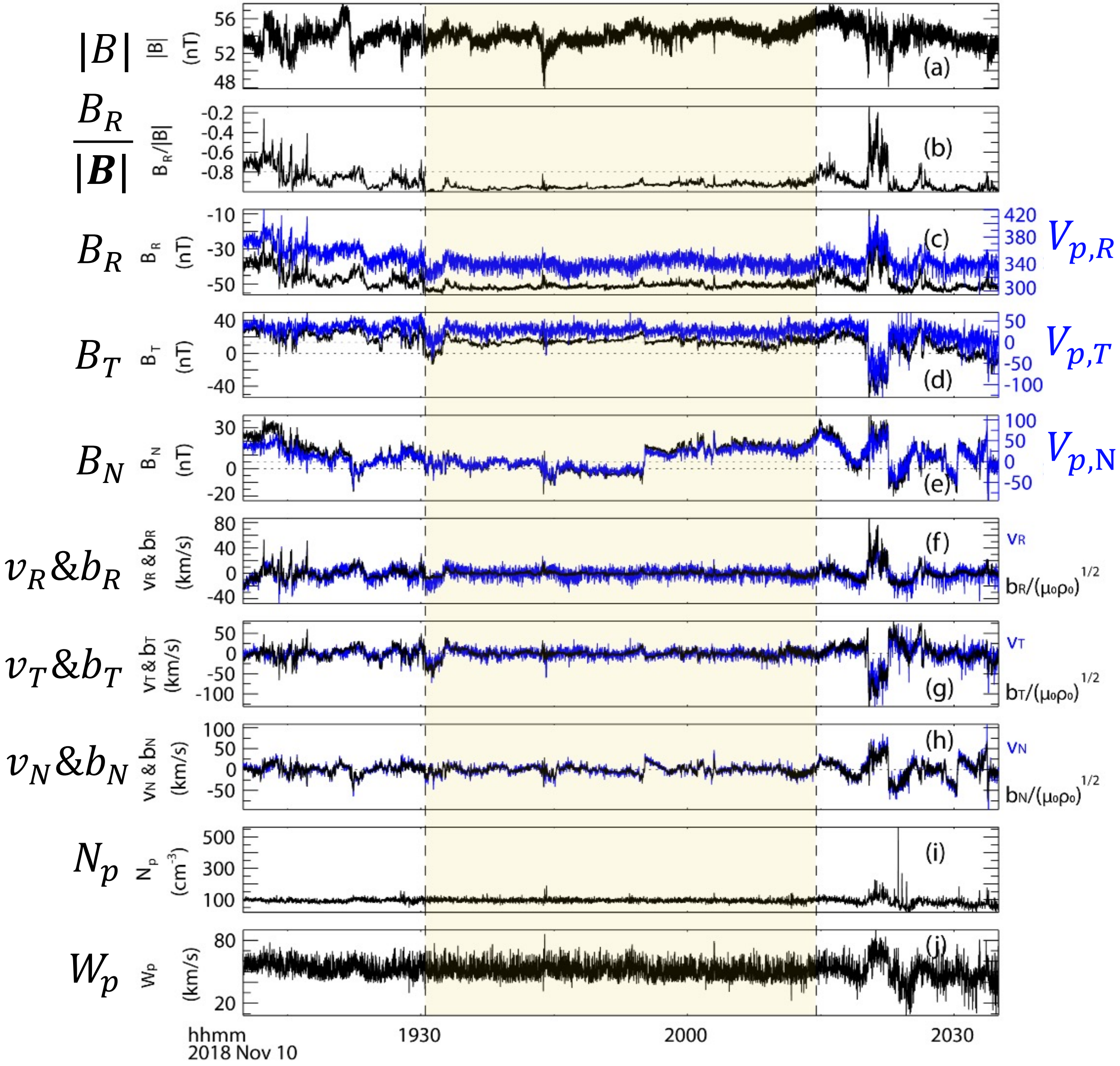

Dataset

- The first *PSP* encounter: 31 Oct. to 12 Nov. 2018.
- Heliocentric distance: between 0.166 and 0.277 AU.

Interval selection criteria

(1) Sub-Alfvénic perturbations ($\boldsymbol{v} \ll \boldsymbol{V_A}$ and $\boldsymbol{b} \ll \boldsymbol{B}_0$)

(2) Large normalized radial magnetic field ($\frac{|B_R|}{|\boldsymbol{B}|} > 0.8$)

(3) High electromagnetic planarity > +0.8

(4) > 20 minutes in length

15 events are identified.

siqi.zhao@desy.de

Mode decomposition methods

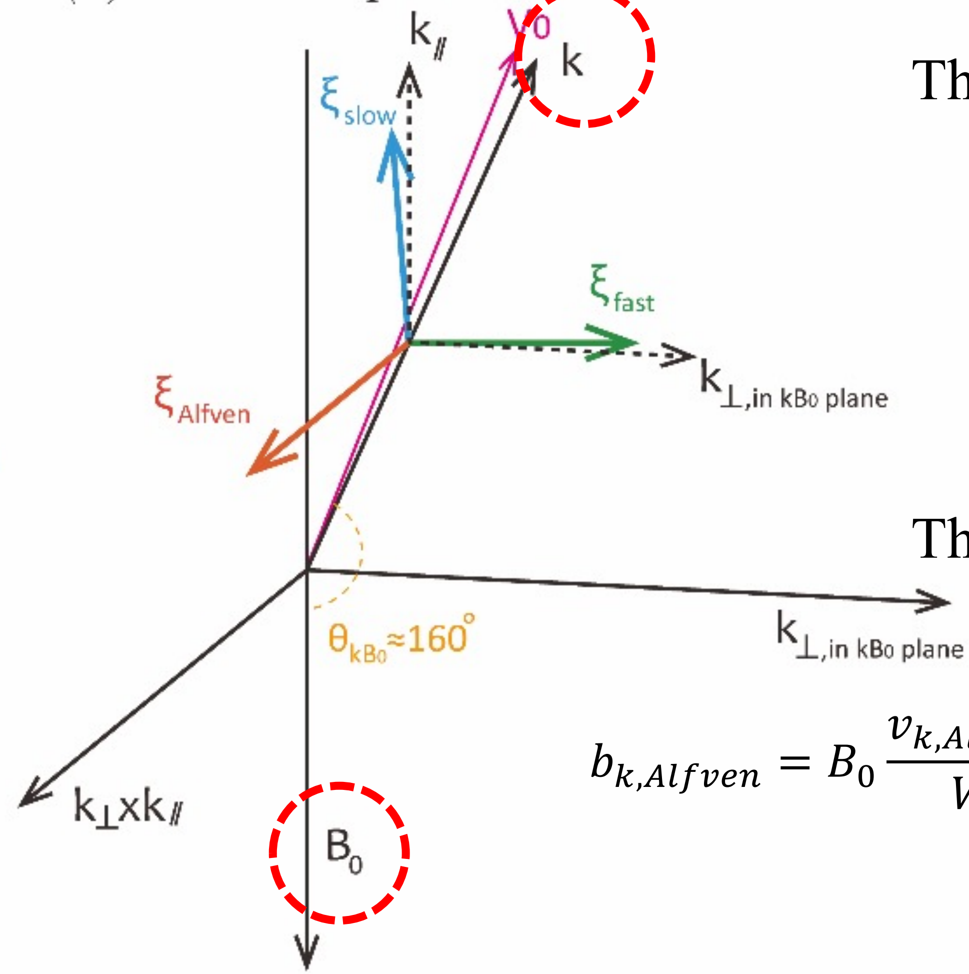

Singular value decomposition $\Rightarrow$ wavevectors $\boldsymbol{k}$

The displacement vectors $\boldsymbol{\xi}$ are expressed as (Cho & Lazarian 2003)

$$\xi_{Alfven} = \widehat{\boldsymbol{k}}_{\perp} \times \widehat{\boldsymbol{k}}_{\parallel}, (1)$$

$$\xi_{slow} \propto \left(-1 + \alpha - \sqrt{D}\right) k_{\parallel} \widehat{\boldsymbol{k}}_{\parallel} + \left(1 + \alpha - \sqrt{D}\right) k_{\perp} \widehat{\boldsymbol{k}}_{\perp}, (2)$$

$$\xi_{fast} \propto \left(-1 + \alpha + \sqrt{D}\right) k_{\parallel} \widehat{\boldsymbol{k}}_{\parallel} + \left(1 + \alpha + \sqrt{D}\right) k_{\perp} \widehat{\boldsymbol{k}}_{\perp}. (3)$$

The phase-space velocity, magnetic field, and density are given by

$$\boldsymbol{v}_k = \boldsymbol{v}_{k,Alfven} + \boldsymbol{v}_{k,slow} + \boldsymbol{v}_{k,fast}, (4)$$

$$b_{k,Alfven} = B_0 \frac{v_{k,Alfven}}{V_A}; \quad b_{k,slow} = B_0 \frac{v_{k,slow}}{c_{slow}} \left|\widehat{\boldsymbol{B}}_{\boldsymbol{0}} \times \hat{\xi}_{slow}\right|; \quad b_{k,fast} = B_0 \frac{v_{k,fast}}{c_{fast}} \left|\widehat{\boldsymbol{B}}_{\boldsymbol{0}} \times \hat{\xi}_{fast}\right|, (5)$$

$$N_k = N_{k,slow} + N_{k,fast} = N_0 \frac{v_{k,slow}}{c_{slow}} \widehat{\boldsymbol{k}} \cdot \hat{\xi}_{slow} + N_0 \frac{v_{k,fast}}{c_{fast}} \widehat{\boldsymbol{k}} \cdot \hat{\xi}_{fast}. (6)$$

Part IV

The comparison of magnetic power

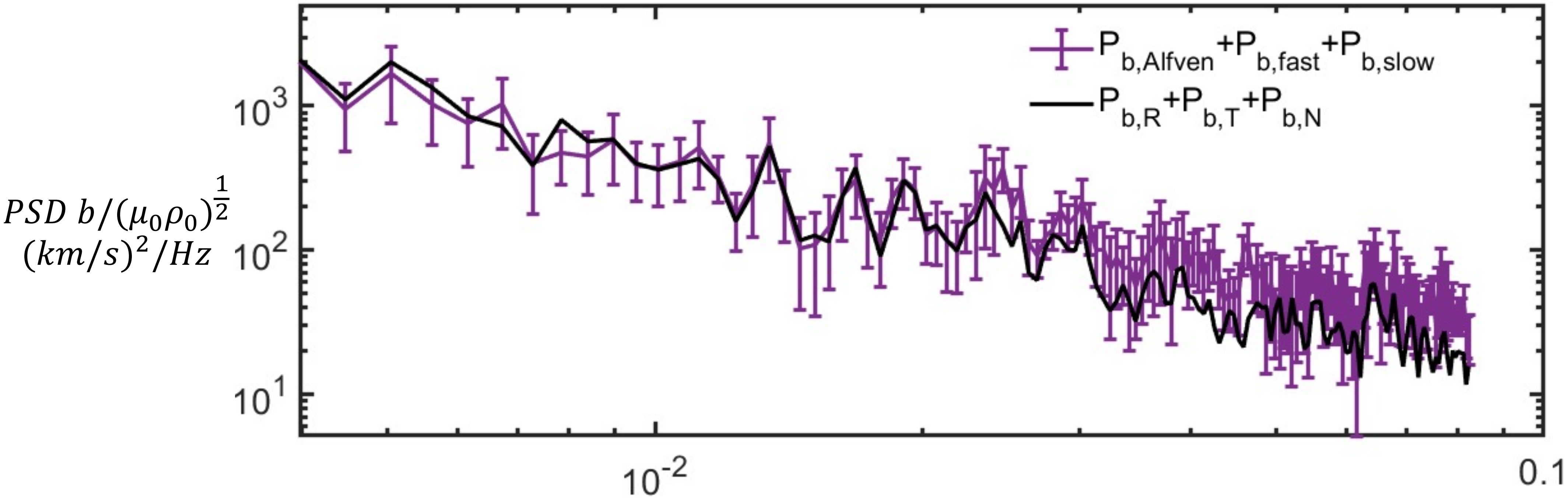

- $P_{b,obs} = P_{b,R} + P_{b,T} + P_{b,N}$: observed magnetic power
- $P_{b,3modes} = P_{b,Alfven} + P_{b,fast} + P_{b,slow}$: magnetic power from decomposition analysis

$$\boldsymbol{P_{b,obs} \sim P_{b,3modes}}$$

Confirming the validity of mode decomposition procedure.

Part IV

Kinetic, magnetic, and density power of each MHD mode

(a) **Total power**

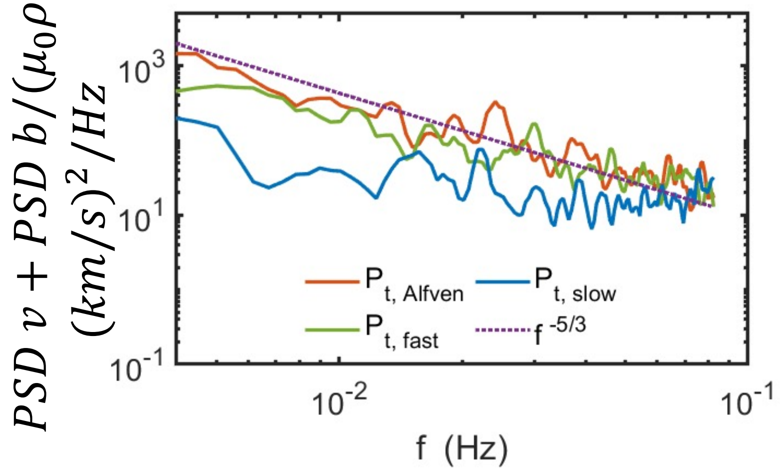

(b) **Kinetic power**

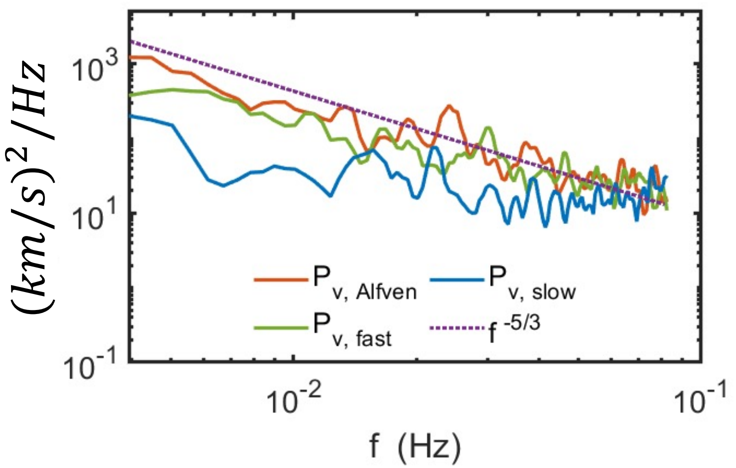

$$P_{KEm} = 100\%\times\frac{\sum_f |U_{f,m}(\boldsymbol{v})|^2}{\sum_{f,m}(|U_{f,m}(\boldsymbol{b})|^2+|U_{f,m}(\boldsymbol{v})|^2)}$$

$$P_{MEm} = 100\%\times\frac{\sum_f |U_{f,m}(\boldsymbol{b})|^2}{\sum_{f,m}(|U_{f,m}(\boldsymbol{b})|^2+|U_{f,m}(\boldsymbol{v})|^2)}$$

(c) **Magnetic power**

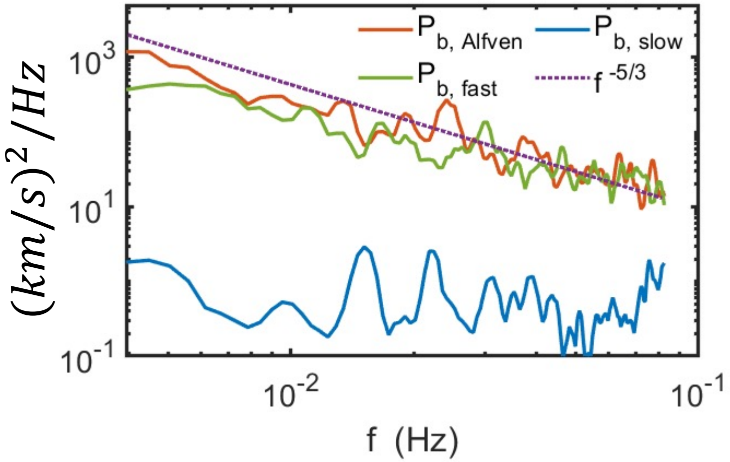

$P_{MEf} \gg P_{MEs}$

(d) **Density power**

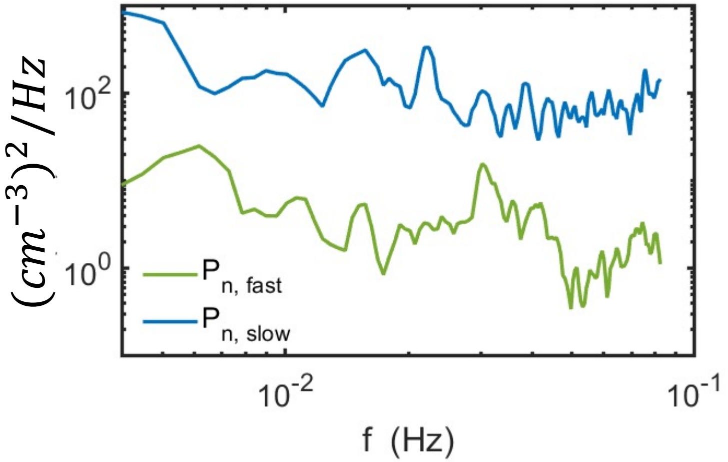

$P_{n,slow} \gg P_{n,fast}$

- **Alfvén mode**: $P_{KEA}\sim P_{MEA}\sim 31\%$
- **Fast mode**: $P_{KEf}\sim 17\%;\ P_{MEf}\sim 16\%$
- **Slow mode**: $P_{KEs}\sim 5\%;\ P_{MEs} \ll 1\%$

Part IV

Contributions to magnetic and density compressibility

—Direct observations —Fast mode —Slow mode —electron density QTN

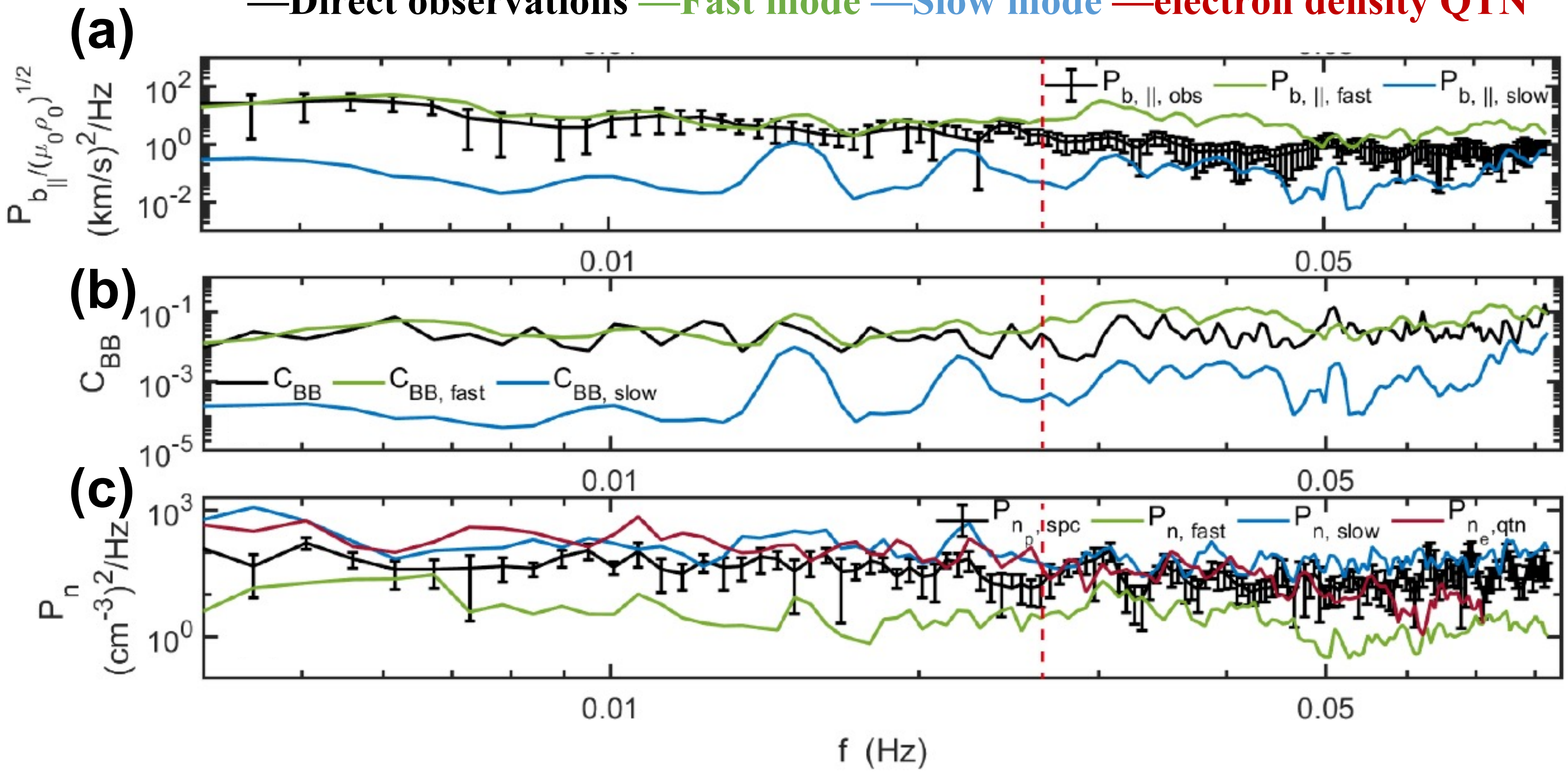

$P_{b,\parallel,fast} \sim P_{b,\parallel,obs} \gg P_{b,\parallel,slow}$

Fast modes provide most of $\delta B_\parallel$.

$C_{BB,fast} \sim C_{BB} \gg C_{BB,slow}$

Fast modes dominate magnetic compressibility.

$P_{n,slow} \sim P_{n_e,qtn} > P_{n_p,spc} \gg P_{n,fast}$

Slow modes dominate density compressibility.

$$C_{BB} = \left(\frac{\delta|\boldsymbol{B}|}{|\delta \boldsymbol{B}|}\right)^2, \quad C_{BB,fast} = \frac{P_{b,\parallel,fast}}{P_{b,3modes}}, \quad \text{and} \quad C_{BB,slow} = \frac{P_{b,\parallel,slow}}{P_{b,3modes}}$$

The red vertical dashed lines: f = 0.026 Hz.

Part IV

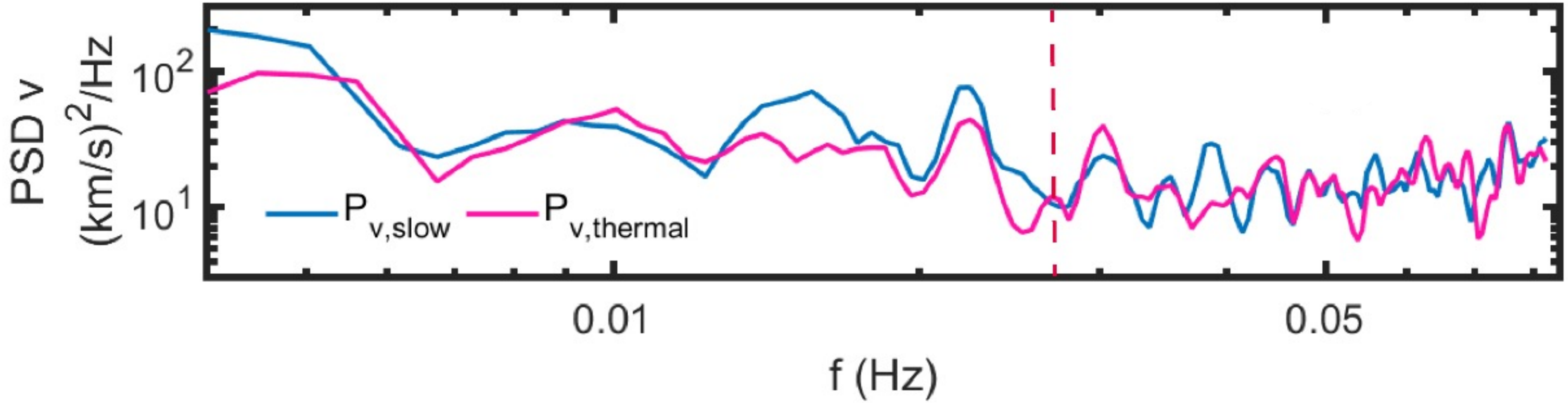

The correlation coefficient between $P_{v,slow}$ and $P_{v,thermal}$ is ~ 0.80.

➤ **Slow mode**: P_{KEs}~5%; $P_{MEs} \ll 1\%$

$\boldsymbol{\xi}_{slow}$ aligns with $\boldsymbol{B_0}$ $\xrightarrow{\frac{\partial \rho}{\partial t} + \nabla \cdot (\rho \boldsymbol{v}) = 0}$ most density fluctuations

Slow modes modulate the motion of plasmas, resulting in thermal energy variations and the inhomogeneous temperature of the plasma.

Part IV

Dispersion relations in the plasma flow frame

$\omega_{obs} = \omega_{sc} - \langle \boldsymbol{k} \rangle \cdot \langle \boldsymbol{V}_p \rangle$

$\langle \theta_{kB_0} \rangle \sim 163^{\circ}$

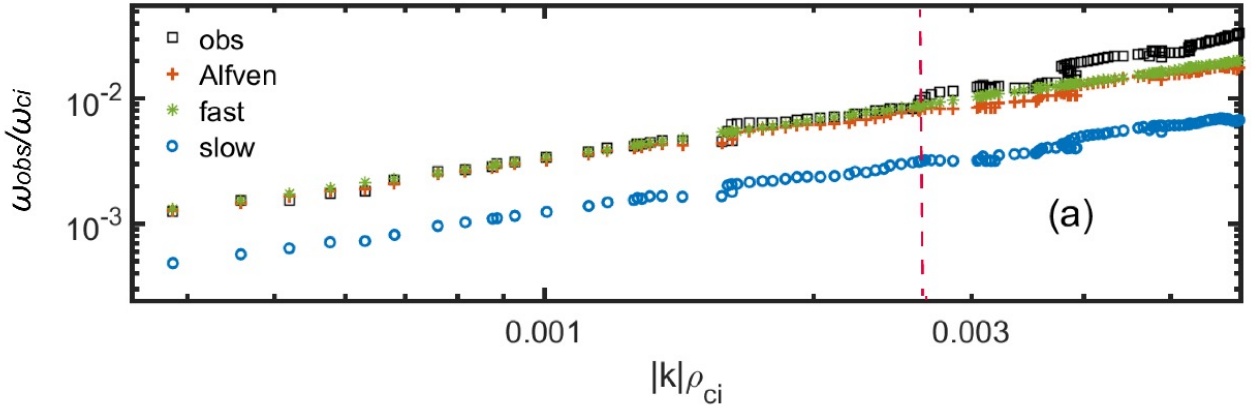

Alfvén- and fast-mode dispersion relations are consistent with **observed results**.

Alfvén and fast modes dominate MHD perturbations.

Based on ideal MHD theory, the wave phase velocity is given by

$$V_{ph,Alfven} = V_A cos\theta_{kB_0},$$

$$V_{ph,\pm}^2 = \frac{1}{2}\left\{(a^2 + V_A^2) \pm [(a^2 + V_A^2)^2 - 4a^2V_A^2cos^2\theta_{kB_0}]^{\frac{1}{2}}\right\}$$

Part IV

Collisionless damping of compressible modes

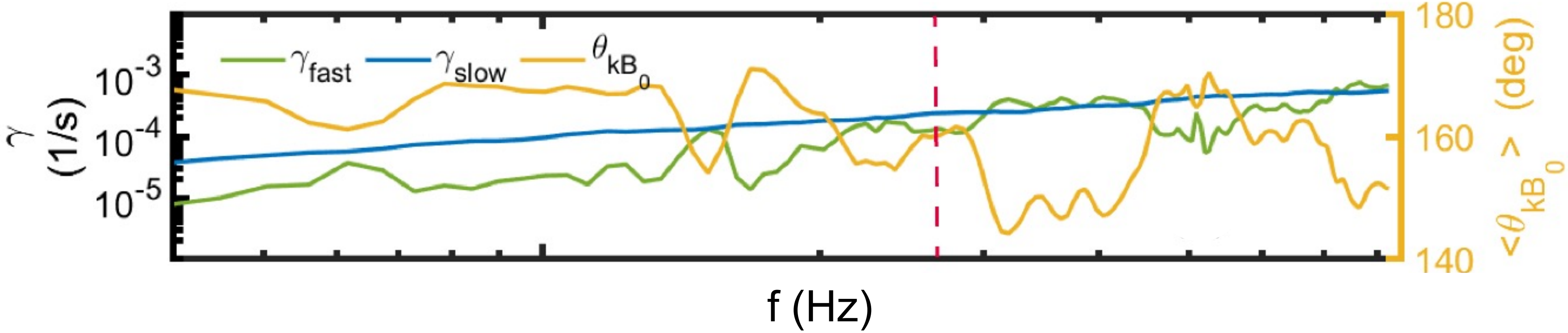

- Both γ_{slow} and γ_{fast} increase with the frequency.
- γ_{slow} is systematically larger than γ_{fast}.

Fast-mode damping rate of ω for $\beta \ll 1$ and $\theta_{kB_0} \sim 1$: $\gamma_{fast} = \omega \frac{\sqrt{\pi\beta}}{4} \frac{\sin^2\theta_{kB_0}}{\cos\theta_{kB_0}} [\sqrt{\frac{m_e}{m_p}} \exp\left(-\frac{m_e}{m_p \beta \cos^2\theta_{kB_0}}\right) + 5\exp(-\frac{1}{\beta \cos^2\theta_{kB_0}})]$

(Ginzburg 1961; Yan & Lazarian 2004; Suzuki et al. 2006)

Slow-mode damping rate (Galeev and Sudan 1983): $\gamma_{slow} = \frac{|k|a}{2|\cos\theta_{kB_0}|} (\frac{1}{8}\pi \frac{m_e}{m_p})^{\frac{1}{2}} \left(1 - \frac{\cos2\theta_{kB_0}[\left(\frac{a^2}{V_A^2}\right)\cos2\theta_{kB_0} - 1]}{[1 + \frac{a^4}{V_A^4} - 2(\frac{a^2}{V_A^2})\cos2\theta_{kB_0}]^{\frac{1}{2}}}\right)$

Part IV

Collisionless damping of compressible modes

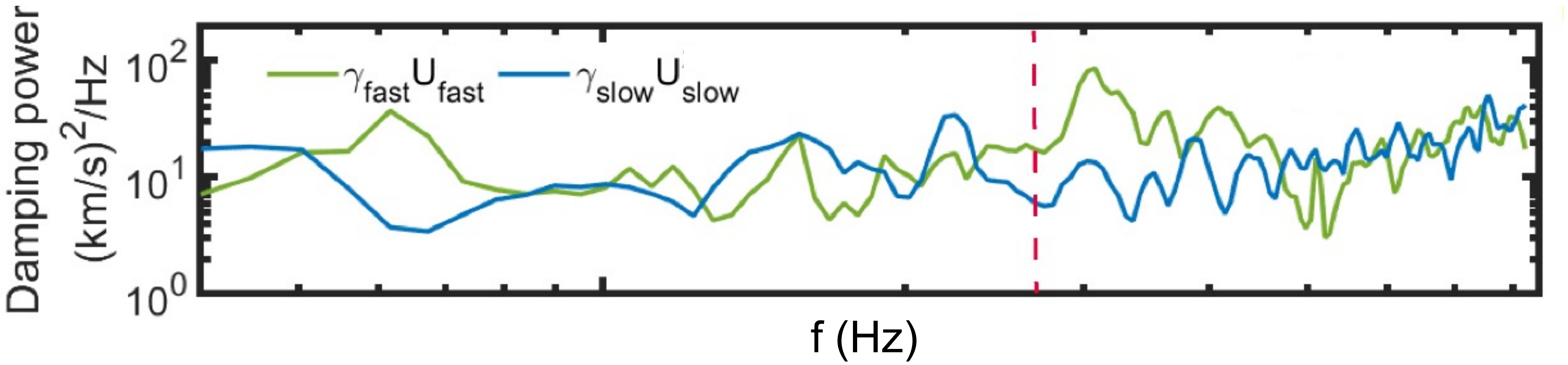

Wave energy damping rate

$\epsilon_{slow} = \int \gamma_{slow} U_{slow}\, df \sim 2.74\times10^5$ J kg^{-1}s^{-1}

$\epsilon_{fast} = \int \gamma_{fast} U_{fast}\, df \sim 2.66\times10^5$ J kg^{-1}s^{-1}

$\epsilon_{slow} \sim \epsilon_{fast} \sim$ heating rate $\sim 2\times10^5$ J kg^{-1}s^{-1}

(Bandyopadhyay et al. 2020)

Part V: Conclusions

- The radial-field solar wind has a high degree of Alfvénicity (~45%-83%), whereas the often-neglected **fast modes (~16%-43%) dominate over** slow modes (~1%-19%). $P_{MEA}{\sim}P_{KEA}{\sim}29\%$; $P_{KEf}{\sim}P_{MEf}{\sim}17.5\%$. $P_{KEs}{\sim}7\%$; $P_{MEs} \ll 1\%$.
- All our events show that **fast modes** provide most of the parallel components of the magnetic field, dominating magnetic compressibility. **Slow modes** provide most of the density fluctuations, dominating density compressibility.
- Slow modes modulate the motion of plasmas, leading to thermal energy variations and the inhomogeneous temperature of the plasma.
- The energy damping rate of compressible modes is comparable to the solar wind heating rate from simulations.

Thanks for your attention!

siqi.zhao@desy.de

References:

Bandyopadhyay, R., Goldstein, M. L., Maruca, B. A., et al. 2020, The Astrophysical Journal Supplement Series, 246, 48

Chen, C. H. K., Bale, S. D., Bonnell, J. W., et al. 2019, The Astrophysical Journal Supplement Series, 246, 53

Cho, J., & Lazarian, A. 2003, Mon Not R Astron Soc, 345, 325

Dobrowolny, M., Mangeney, A., & Veltri, P. L. 1980, Solar and Interplanetary Dynamics, 83, 26

Galeev, A. A., & Sudan, R. N. (1983). Basic plasma physics. Plasma Physics, 1

Glassmeier, K., Motschmann, U., & Stein, R. 1995, Annales Geophysicae, 13, 76

Ginzburg, V. L. 1961, Propagation of Electromagnetic Waves in Plasma (New York: Gordon & Breach)

Makwana, K. D., & Yan, H. 2020, Physical Review X, 10, 031021

Suzuki, TK., Yan, H., Lazarian, A., & Cassinelli, JP. 2006, The Astrophysical Journal, 640, 1005

Verscharen, D., Klein, K. G., & Maruca, B. A. 2019, Living Reviews in Solar Physics, 16, 5

Yan, H. & Lazarian 2004, The Astrophysical Journal, 614, 757